March 1992

Mathematical Analysis of the Joint Motion of Redundant Robots Under Pseudo-Inverse Control

Shengwu Luo
Purdue University School of Electrical Engineering

Shaheen Ahmad
Purdue University School of Electrical Engineering

Mathematical Analysis of the Joint Motion of Redundant Robots Under Pseudo-Inverse Control

Shengwu Luo
Shaheen Ahmad

TR-EE 92-12
March 1992

MATHEMATICAL ANALYSIS OF THE JOINT DRIFT MOTION OF REDUNDANT ROBOTS UNDER PSEUDO-INVERSE CONTROL

Shenpwu Luo and Shaheen Ahmad

Real-Time Robot Control Laboratory
School of Electric Engineering, Purdue University
West Lafayette, IN 47907, USA

Abstract

Redundant robots that are kinematically controlled using Jacobian pseudo-inverses may not have repeatable joint motions, when the end-effector traces a closed path in the workspace. This phenomenon is known as joint drift. The joint drift problem was initially observed and analyzed by Klein and Huang[10]. Shamir and Yomdin[15] also analyzed this problem using differential geometric approach. Klein and Kee[11] observed through numerical experiments that the drift had predictable properties. In this paper we present a measure of the drift motion, we show this measure is useful for predicting the stability properties of drifts. We further show that this measure of drift does indeed exhibit the properties numerically observed by Klein and Kee.

I. Introduction

If the end-effector of a kinematically redundant robot is made to trace a closed path in the workspace by using a kinematical motion rate control scheme utilizing the Jacobian pseudo-inverse, the path in the joint space is not necessarily closed. This phenomenon of non-repeatability of joint motion while using Jacobian pseudo-inverse control has been known for a while[10]. Recently Klein and Kee[11] studied the properties of the drift motion (the non-repeatability of the joint motion) by performing numerical experiments. They showed that the drift has predictable, numerically stable limits in some situations. Klein and Huang originally observed the drift phenomenon[10] and analyzed the non-repeatability phenomenon for a three degree-of-freedom revolute joint planar arm in terms of the integrability condition of a Pfaffian differential equation. Shamir and Yomdin [15] formulated the non-repeatability problem of redundant manipulators by the existence of an integral surface of the distribution spanned by the matrix J^+ (the pseudo-inverse of the Jacobian J). Under this differential geometric framework the application of Frobenius' theorem yields a "Lie bracket condition" (LBC), which provides us with a mathematical criterion to check the repeatability, that is, when the drift does not exist. However the LBC does not tell us the behavior of the drift if it exists. Recently Bay [2] propoaed the uae of Poincare return map to approximate and analyze the drift motion. Luo and

Ahmad[12] proposed a measure of the drift which is easy to compute and easy to use in the two dimensional workspace. Phase portrait analysis of the measure, used in[12], shows the limit behaviors of the drift. This paper presents the generalization of the measure of the drift into higher dimensional workspace for redundant robots. In section II of this paper the drift is formulated as a line integral on a manifold in the work space. It is then shown that the drift motion can be expressed by the integral of the Lie brackets of the Jacobian pseudo-inverse J+. In section III a measure of the drift density is defined and expressed as the projection of the Lie brackets of J^+ on the self-motion space. The computation of the drift density is considered in section IV. It is shown that the Lie bracket of J^+ can be replaced by the Lie bracket of J^T, this simplifies the computation of the drift density. In section V we describe a method for representing the self-motion space by a "chart". The drift density is represented by the linear combination of the tangent vectors of this chart. In section VI the stability analysis of the drift motion is presented, a theorem on the stability of drift is also given. Simulations are given in section VII. Conclusions of the paper are given in section VIII.

II. The Formulation of Drift

Consider a redundant manipulator with its joint space Q in R" and its work space X in R^m. The work space velocities and the joint space velocities are related by an m by n Jacobian J :

$$\dot{x} = J\,\dot{q} \tag{1}$$

The Jacobian pseudo-inverse J^+ is used to determine the minimum norm joint rates as,

$$\dot{q} = J^+\,\dot{x} \quad | \quad q(0)=q_0 \tag{2}$$

Let N_j be the n by (n−m) matrix, whose columns are the basis vectors of the null space of J, such that,

$$J\,N_J=0 \quad \text{and then} \quad N_J^T\,J^+=0\,.$$

Hence, the joint motion governed by (2) are characterized by

$$N_J^T\,\dot{q}=0\,. \tag{3}$$

This constraint on the joint motion is said to be "nonholonomic"[3], if the equation (3) is not completely integrable for the joint variable q. The non-integrability of the joint motion under pseudo-inverse Jacobian control has been established[15]. As the constraint (3) is equivalent to (2), this will imply that if (2) is not integrable, that is if joint drift motion exists, then the redundant robot under pseudo-inverse control will be said to be non-holonomic. The joint drift phenomenon will now be addressed in the sections below.

The robot joint position governed by (2) can be found from the following integral equation when the end-effector of the manipulator traces a parametrized path x(t):

$$q(t_1) = \int_0^{t_1} J^+(q(t))\dot{x}dt \quad | \quad q(0)=q_0 \tag{4}$$

Thia expression enables us to mathematically describe the drift by the following definition.

Definition 1 : The "drift" of the joints $dr \in \mathbb{R}^n$ during pseudo-inverse control is defined as the difference of the joint position vector undergoing one cycle of the path ∂W in the work space in the time interval $t \in [t_1, t_1+T]$. The drift is a vector-valued line integral of J^+ along a closed path ∂W :

$$dr(\partial W) \triangleq q(t_1+T)-q(t_1) \;\big|_{x(t_1+T)=x(t_1)} = \oint_{\partial W} J^+(q)dx \; . \qquad \diamond \qquad (5)$$

Differentiable manifold terminology will be used further in this paper. The detailed concepts of exterior product, differential form, integral on a manifold, integral of form and Stokes' formula can be found in [4, 6, 16]. In differential geometric formulation the term J^+dx in eq(5) is an (vector-valued) 1-form because of $J^+dx=\sum_{i=1}^{m} J^+_i dx_i$, where we denote by J^+_i the i-th column of matrix J^+, then each row of J^+dx is an 1-form. Therefore the definition 1 can be restated as an (vector-valued) "integral of 1-form". Now we are ready to apply the Stokes' formula, which yields an equivalent expression of a surface integral for $dr(\partial W)$. Precisely speaking, if D is a compact oriented 2-dimensional manifold with boundary ∂W and orientation α, then,

$$dr(\partial W) = \oint_{\partial W} J^+dx = \int_{W^\alpha} d(J^+dx) \qquad (6)$$

where, $d(J^+dx)$ is a differential 2-form, which can be calculated by :

$$d(J^+dx) = \sum_{i=1}^{m} dJ^+_i \wedge dx_i = \sum_{i=1}^{m}\sum_{\substack{j=1 \\ j\neq i}}^{m} \frac{\partial J^+_i}{\partial x_j} dx_j \wedge dx_i = \sum_{i<j} \frac{\partial J^+_i}{\partial x_j} dx_j \wedge dx_i \qquad (7)$$

where the symbol $\wedge$ denotes the "exterior or the wedge product", and $\sum_{i<j}$ denotes $\sum_{i=1}^{m}\sum_{\substack{j=1 \\ j\neq i}}^{m}$. As an example with $m=4$, the pairs (i,j) in the summation all come from the set $\{(i,j) \mid i<j\} = \{(1,2), (1,3), (1,4), (2,3), (2,4)$ and $(3,4)\}$. Applying eq(5) to the work space of m-dimension, i.e., $x \in \mathbb{R}^m$, yields the next proposition.

Proposition 1: On a 2-dimensional manifold W in an m-dimensional workspace, when the end-effector follows a loop ∂W, which is the boundary of W, the drift motion of a redundant manipulator controlled by pseudo-inverse can be expressed as a sum of $\binom{m}{2}$ integrals of 2-form:

$$dr(\partial W)=\sum_{i<j} \int_{W^\alpha} [J^+_i, J^+_j] dx_i \wedge dx_j \; . \qquad \diamond \qquad (8)$$

The following lemma will greatly simplify the proof of Proposition 1.

Lemma *1:* For $x \in \mathbb{R}^m$ and $dJ^+=\sum_{j=1}^{m} \frac{\partial J^+}{\partial x_j} dx_j$. The 2-form in eq(7) can be expanded as

$$d(J^+dx) = \sum_{i=1}^{m} dJ^+_i \wedge dx_i = \sum_{i=1}^{m-1} \sum_{j=i+1}^{m} \left(\frac{dJ^+_j}{dx_i} - \frac{dJ^+_i}{dx_j} \right) dx_i \wedge dx_j \; . \qquad \diamond \qquad (9)$$

Proof: In light of the properties of exterior product we have, $dx_k \wedge dx_k = 0$, and, $dx_i \wedge dx_j = -dx_j \wedge dx_i$, if $j \neq i$. Then it is easy to show that eq(9) is true for $m=2$, by directly applying eq(7) :

$$d(J^+dx) = dJ^+_1 \wedge dx_1 + dJ^+_2 \wedge dx_2$$

$$= \frac{dJ^+_1}{dx_2} dx_2 \wedge dx_1 + \frac{dJ^+_2}{dx_1} dx_1 \wedge dx_2 = \left(\frac{dJ^+_2}{dx_1} - \frac{dJ^+_1}{dx_2} \right) dx_1 \wedge dx_2 \tag{10}$$

Now assume that the induction hypothesis **eq(9)** holds for **m=k-1,** we can show it holds for **m=k.** Since the summation operator can be decomposed as

$$\sum_{i=1}^{k} \sum_{\substack{j=1 \\ j \neq i}}^{k} = \sum_{i=1}^{k-1} \sum_{\substack{j=1 \\ j \neq i}}^{k} + \sum_{j=1}^{k} \Big|_{i=k} = \sum_{i=1}^{k-1} \sum_{\substack{j=1 \\ j \neq i}}^{k-1} + \sum_{i=1}^{k-1} \Big|_{j=k} + \sum_{j=1}^{k} \Big|_{i=k} \ . \tag{11}$$

Applying this decomposition to **eq(7)** yields,

$$\begin{aligned} d(J^+ dx) &= \sum_{i=1}^{k} \sum_{\substack{j=1 \\ j \neq i}}^{k} \frac{\partial J^+_i}{\partial x_j} dx_j \wedge dx_i \\ &= \sum_{i=1}^{k-1} \sum_{\substack{j=1 \\ j \neq i}}^{k-1} \frac{\partial J^+_i}{\partial x_j} dx_j \wedge dx_i + \sum_{i=1}^{k-1} \frac{\partial J^+_i}{\partial x_k} dx_k \wedge dx_i + \sum_{j=1}^{k} \frac{\partial J^+_k}{\partial x_j} dx_j \wedge dx_k \\ &= \sum_{i=1}^{k-1} \sum_{\substack{j=1 \\ j \neq i}}^{k-1} \frac{\partial J^+_i}{\partial x_j} dx_j \wedge dx_i + \sum_{j=1}^{k-1} \left(\frac{\partial J^+_i}{\partial x_k} - \frac{\partial J^+_k}{\partial x_j} \right) dx_k \wedge dx_i \ . \end{aligned} \tag{12}$$

The first term of the above **by** assumption is just the expression of **eq(9)** for **m=k-1,** hence the above equation reduces to

$$\sum_{i=1}^{k-2} \sum_{j=i+1}^{k-1} \left(\frac{dJ^+_j}{dx_i} - \frac{dJ^+_i}{dx_j} \right) dx_i \wedge dx_j + \sum_{j=1}^{k-1} \left(\frac{\partial J^+_i}{\partial x_k} - \frac{\partial J^+_k}{\partial x_j} \right) dx_k \wedge dx_i \ . \tag{13}$$

First notice that the summation on the right hand side of **eq(9)** for **m=k** can be decomposed as,

$$\sum_{i=1}^{k-1} \sum_{j=i+1}^{k} = \left(\sum_{i=1}^{k-2} + \Big|_{i=k-1} \right) \left(\sum_{j=i+1}^{k-1} + \Big|_{j=k} \right) = \sum_{i=1}^{k-2} \sum_{j=i+1}^{k-1} + \sum_{j=i+1}^{k-1} \Big|_{i=k-1} + \sum_{i=1}^{k-1} \Big|_{j=k} \ . \tag{14}$$

The second term vanishes since the value of the superscript is less than the subscript. From **eq(14)** we see that the first term represents **eq(9)** for **m=k-1** and the third term is the additional term needed to make **eq(14)** the summation for **m=k, as** expressed **by** (9). Therefore the left hand side of **eq(14)** is the expression of $d(J^+ dx)$ for $x \in \mathbb{R}^m$ and **m=k.** This verifies the lemma. ●

Now we return to Proposition 1.

Proof of Proposition 1 : Expanding the derivative of J^+_i **by** $\frac{\partial J^+_i}{\partial x_j} = \frac{\partial J^+_i}{\partial q} \frac{\partial q}{\partial x_j}$, and recalling that $dq = J^+ dx$ implies that, $\frac{\partial q}{\partial x_j} = J^+_j$. Then we have the term in **eq(13)** equals to

$$\left(\frac{dJ^+_j}{dx_i} - \frac{dJ^+_i}{dx_j} \right) = \frac{\partial J^+_j}{\partial q} \frac{\partial q}{\partial x_i} - \frac{\partial J^+_i}{\partial q} \frac{\partial q}{\partial x_j} = [J^+_i, J^+_j] \ . \tag{15}$$

This is exactly the integrand in **eq(8).** ■

Ezample : The drift for m=3 is given by **eq(8):**

$$dr(\partial W) = \int_{W^a} \{ [J^+_1, J^+_2] dx_1 \wedge dx_2 + [J^+_2, J^+_3] dx_2 \wedge dx_3 + [J^+_3, J^+_1] dx_3 \wedge dx_1 \}$$

◇

The computation of the integration of differential forms is carried out by the change of coordinates that transforms the integration of differential form into a multiple integration on a planar area attached with orthonormal coordinates **(u,v)**. This is formally stated in the next corollary.

Corollary: Let $\mathbf{g}=(g_1,\ldots,g_m): D\rightarrow W$ be a regular transformation from area D in **(u,v)** plane into workspace W of x, such that $x_i=g_i(u,v)$, $i=1,\ldots,m$. Then the drift defined by **eq(8)** can be calculated by,

$$dr(\partial W)=\sum_{i<j}\int_{W^o}[J^+_i,J^+_j]dx_i\wedge dx_j=\sum_{i<j}\int_D\left[[J^+_i,J^+_j]\frac{\partial(g_i,g_j)}{\partial(u,v)}\right]du\,dv \qquad (16)$$

where, $\dfrac{\partial(g_i,g_j)}{a(\sim,.)}-\det\begin{vmatrix}\dfrac{\partial g_i}{\partial u} & \dfrac{\partial g_i}{\partial v}\\ \dfrac{\partial g_j}{\partial u} & \dfrac{\partial g_j}{\partial v}\end{vmatrix}$.

The right hand side of above expression is reached by assigning a change of variables in **eq(8).** (See the integral on manifolds formula (7-10) and the example 6 in p.261 of [6]).

III. Definition and Computation of The Drift Density

The drift defined in **eq(5)** is a line integration on the closed path in the work space. In light of the generalized Stokes' theorem on a manifold, this integral can be expressed as a surface integral, which implies that the drift is an area sum of an object that is analogous to the curl in the 3-dimensional field theory. Thus it naturally motivates a measure of drift density, which is easy to compute and should be easy to use in order to show the limit loop phenomenon of the joint motion repeatability.

Recall that the drift given by eq(8) lies on the self-motion manifold, thus the infinitesimal drift motion will be a vector on the tangent space of the self-motion manifold. This motivates the following definition of drift density.

Definition 2: Let **ker(J)** be the null space of the Jacobian J. The projection operator onto **ker(J)** is denoted by $\mathbf{P}_{\mathbf{ker(J)}}$. The "drift density at point q" **dd(q)** is the projection of drift (area) derivative onto the null space of J at point q. Here the drift derivative is a ratio of the path integral of **eq(8)** on an infinitesimal loop over the area of the surface surrounding the infinitesimal loop. This is a function of the joint angles q, **i.e.,**

$$\textbf{drift density}, \quad \mathbf{dd(q)}\triangleq\mathbf{P}_{\mathbf{ker(J)}}\left\{\lim_{\mathbf{diamD}\rightarrow 0}\frac{1}{\mathbf{area(D)}}\mathbf{dr}(\partial W)\right\} \qquad \text{o} \quad (17)$$

From Definition 2 and **eq(16)** the drift **density for the m-dimensional work**space can be **expressed** as a sum of $\binom{m}{2}$ terms :

$$\textbf{drift density}, \quad \mathbf{dd(q)}=\mathbf{P}_{\mathbf{ker(J)}}\left\{\lim_{\mathbf{diamD}\rightarrow 0}\frac{1}{\mathbf{area(D)}}\sum_{i<j}\int_D[J^+_i,J^+_j]\frac{\partial(g_i,g_j)}{\partial(u,v)}\,\mathbf{dudv}\right\} \qquad (18)$$

Proposition 2: Let $\mathbf{g}=(g_1,\cdots,g_m): D\rightarrow W$ be a regular transformation from area D in (u,v) plane into workspace W of $\mathbf{x}$, such that $x_i=g_i(u,v)$, $i=1,\ldots,m$. Then the drift density defined by eq(17) can be computed by,

$$dd(q) = (I_n - J^+J)\left\{\sum_{i=1}^{m-1}\sum_{j=i+1}^{m}[J^+_i, J^+_j]\,\frac{\partial(g_i,g_j)}{\partial(u,v)}\right\}, \tag{19}$$

where, $\dfrac{\partial(g_i,g_j)}{\partial(u,v)} = \det\begin{vmatrix} \dfrac{\partial g_i}{\partial u} & \dfrac{\partial g_i}{\partial v} \\ \dfrac{\partial g_j}{\partial u} & \dfrac{\partial g_j}{\partial v} \end{vmatrix}$ accounts for the transformation between the coordinates.

0

The proof is obtained from the integral mean value lemma stated in the below.

Lemma 2: (p.266 in [6]) If f is continuous on an open set $D\subset R^m$ containing x_0, then,

$$f(x_0)= \lim_{\text{diam}D\rightarrow 0}\frac{1}{V_m(D)}\int_D f(x)dV_m(D)$$

where $V_m(D)$ is the measure of the m-dimensional manifold D. If the coordinate system used for D is chosen to be the standard Cartesian coordinates: $x_1,\cdots,x_m$, then $dV_m(D)=dx_1.....dx_m$. ◇

For the differential form, more exactly, we have following localization lemma, which is proved[8] from the mean value lemma.

Lemma 2A **(p.70, [8])** Let w be a **(k-1)** form that is continuously differentiable on the k dimensional smooth manifold $M\subset R^n$, and {D) is a set of almost smoothly bordered pieces in M converging to **x**, then

$$\lim_{D\rightarrow x}\frac{1}{V(D)}\int_{\partial D}\omega = d\omega(x;J_n^{(k)}(x)).$$

Where $V(D)$ is the volume of D, the volume by definition is a measure of D that is invariant under isometries; and $J_n^{(k)}$ is a unit-k-vector, strictly collinear † to the tangent space of M in *x*. ◇

Proof of proposition 2 : The change of coordinates transforms the integration of differential form into a multiple integration on a planar area attached with orthonormal coordinates. This multiple integral has the value given in (16). The desired formula of (18) follows immediately by applying the Lemma 2. ∎

The Lemma 2A is the more rigorous statement of the part in the braces of (18) given in Proposition 2. Lemma 2A also shows that the differential k-form dw plays a role of the generalized curl. Specifically for **k=2,** the surface integral of dw is equal to the line integral of w, **i.e.,** dw is an area density, this motivated us to call **dd(q)** as the drift density. The drift density given in Definition 2 will allow us to easily set up the phase portrait analysis of the drift motion, this will be illustrated by examples in section VII.

---

† **Any two subspace in a linear** vector **space are said to be collineru if they span the same subspace; they are said** to **be strictly collineru if they also agree in their orientation.**

IV. The Drift Formula Expressed by J^T Instead of J^+

For the convenience of calculations we prefer to express the drift density eq(19) by J^T. Next lemma establishes the relationship between Lie-brackets of J^+ and that of J^T, it offers us simplicity in computing the drift density.

Lemma 8: For $x\in\mathbb{R}^m$ and $J^+=J^T(JJ^T)^{-1}$, we denote $J^+=J^TA$ for brevity, where $A=(JJ^T)^{-1}$ is an $m\times m$ symmetric invertible matrix. We also denote the vector A_i by the i-th column of A and a_{ij} by the ij-th entry of A in the below. Then,

$$[J^+_i,J^+_j]=\sum_{l_1=1}^{m-1}\sum_{l_2=l_1+1}^{m}[J^T_{l_1},J^T_{l_2}]\ \det\begin{bmatrix}a_{l_1i} & a_{l_1j}\\ a_{l_2i} & a_{l_2j}\end{bmatrix}+\ J^T\left(\frac{dA_j}{dx_i}-\frac{dA_i}{dx_j}\right). \qquad \diamond \qquad (20)$$

Proof: We start from calculating the partial derivatives in eq(15),

$$\frac{dJ^+_j}{dx_i}=\frac{dJ^TA_j}{dx_i}=\frac{dJ^T}{dx_i}A_j+J^T\frac{dA_j}{dx_i}=\sum_{l_1}^{m}\frac{dJ^T_{l_1}}{dx_i}\,a_{l_1j}+J^T\frac{dA_j}{dx_i}.$$

In light of $\frac{\partial q}{\partial x_i}=J^+_i=J^TA_i$, above derivative is,

$$\frac{dJ^+_j}{dx_i}=\sum_{l_1}^{m}\frac{\partial J^T_{l_1}}{\partial q}J^TA_i\,a_{l_1j}+J^T\frac{dA_j}{dx_i}=\sum_{l_1}\sum_{l_2}\frac{\partial J^T_{l_1}}{\partial q}J^T_{l_2}\,a_{l_2i}\,a_{l_1j}+J^T\frac{dA_j}{dx_i}.$$

Hence eq(15) equals to

$$\begin{aligned}[J^+_i,J^+_j]&=\sum_{l_1=1}^{m}\sum_{l_2=1}^{m}\frac{\partial J^T_{l_1}}{\partial q}J^T_{l_2}\,(a_{l_2i}\,a_{l_1j}-a_{l_2j}\,a_{l_1i})+J^T\left(\frac{dA_j}{dx_i}-\frac{dA_i}{dx_j}\right)\\&=\sum_{l_1=1}^{m-1}\sum_{l_2=l_1+1}^{m}[J^T_{l_1},J^T_{l_2}]\ \det\begin{bmatrix}a_{l_1i} & a_{l_1j}\\ a_{l_2i} & a_{l_2j}\end{bmatrix}+J^T\left(\frac{dA_j}{dx_i}-\frac{dA_i}{dx_j}\right).\end{aligned}$$

■

The "det" terms in the above expression eq(20) are the determinants formed from elements of the matrix A. We will adopt the concise notation introduced by Gantmacher (p.2, [7]):

$$A\begin{pmatrix}i & j\\ l_1 & l_2\end{pmatrix}=\det\begin{bmatrix}a_{l_1i} & a_{l_1j}\\ a_{l_2i} & a_{l_2j}\end{bmatrix}.$$

The above determinant is called a minor of A of order 2. Similarly, the minor of A of order p can be defined as:

$$A\begin{pmatrix}i_1 & i_2 & \cdots & i_p\\ l_1 & l_2 & \cdots & l_p\end{pmatrix}=\det\begin{vmatrix}a_{i_1l_1} & a_{i_1l_2} & \cdots & a_{i_1l_p}\\ a_{i_2l_1} & a_{i_2l_2} & \cdots & a_{i_2l_p}\\ \cdots & \cdots & & \cdots\\ a_{i_pl_1} & a_{i_pl_2} & \cdots & a_{i_pl_p}\end{vmatrix}$$

Let λ denote an p-tuple of ordered integers:

$$\lambda=(i_1,i_2,\cdots,i_p)\quad|\quad 1\le i_1<i_2<\cdots<i_p\le n\ .$$

It can be shown to further simplify the notation of the p-th order minor by letting $\lambda_1=(i_1,i_2,\cdots,i_p)$ and $\lambda_2=(l_1,l_2,\cdots,l_p)$, then,

$$A\begin{pmatrix}\lambda_1\\ \lambda_2\end{pmatrix} = A\begin{pmatrix}i_1 & i_2 & \cdots & i_p\\ l_1 & l_2 & \cdots & l_p\end{pmatrix}.$$

As A is an inverse matrix, $A=(JJ^T)^{-1}$, all the minors of **A** can be expressed by the minors of the matrix JJ^T. Therefore we can calculate the drift density vector without performing any matrix inversions. Thus we have the following lemma.

Lemma *4*: Let $A=(JJ^T)^{-1}$, then

$$A\begin{pmatrix}i & j\\ l_1 & l_2\end{pmatrix} = A\begin{pmatrix}\lambda_1\\ \lambda_2\end{pmatrix} = (-1)^{(i+j+l_1+l_2)}(JJ^T)\begin{pmatrix}\lambda'_1\\ \lambda'_2\end{pmatrix}/\det(JJ^T). \tag{21}$$

where λ' denotes the complement of n-2 tuple of ordered integers such that after reordering the n-tuple (λ,λ') becomes $(1,2,\ldots,n)$, so $(i,j)'$ is indeed the (n-2)-tuple obtained after deleting the integer i and j from the n-tuple $(1,2,\ldots,n)$, that is, $(i,j)'=(1,2,\ldots,\hat{i},\ldots,\hat{j},\ldots,n)$, where the symbol $\hat{i}$ means that the integer i is deleted from the n-tuple $(1,\ldots,n)$. ***0***

The proof can be found in (p.21, [7]).

Proposition 3: The drift density dd defined by **eq(17)** can be expressed by J^T as a sum of $\binom{m}{2}$ terms of Lie bracket projections and then,

drift density
$$dd = P_{\ker(J)}\left\{\sum_{i=1}^{m-1}\sum_{j=i+1}^{m}[J^+{}_i, J^+{}_j]\frac{\partial(g_i,g_j)}{\partial(u,v)}\right\}$$
$$= \left(I_n - J^T(JJ^T)^{-1}J\right)\sum_{l_1=1}^{m-1}\sum_{l_2=l_1+1}^{m}\left\{[J^T{}_{l_1}, J^T{}_{l_2}]\frac{\partial(g_i,g_j)}{\partial(u,v)}\right.$$
$$\left.\left(\sum_{i=1}^{m-1}\sum_{j=i+1}^{m}(-1)^{(i+j+l_1+l_2)}(JJ^T)\begin{pmatrix}i,j\\ l_1,l_2\end{pmatrix}'\right)\right\}. \tag{22}$$

Where the transformation **g(u,v)** has been defined in Proposition 2. ***0***

Proof : Simply substituting **eq(20)** of the Lemma 3 into the definition **eq(18),** and noticing that $P_{\ker(J)}\{J^T\}=0$, since $P_{\ker(J)}=(I_n-J^+J)$ is the projection onto the null space of J. After rearranging the expression and applying Lemma 4 the desired result is produced. ■

As an example calculation, consider the case with m=2 , since the workspace is planar the coordinates transformation is not necessary, **eq(20)** yields the drift density for the path in a two dimensional work space **as,**

$$dd\,|_{m=2} = (I_n - J^+J)[J^+{}_1, J^+{}_2] = \left(I_n - J^T(JJ^T)^{-1}J\right)[J^T{}_1, J^T{}_2]/\det(JJ^T). \tag{23}$$

For **m=3,** we obtain, the drift density for the path in a three dimensional work space,

$$dd\,|_{m=3} = P_{\ker(J)}\left\{\left((JJ^T)_{31}-(JJ^T)_{32}+(JJ^T)_{33}\right)[J^T{}_1, J^T{}_2]\frac{\partial(g_1,g_2)}{\partial(u,v)}\right.$$
$$+\left((JJ^T)_{11}-(JJ^T)_{12}+(JJ^T)_{13}\right)[J^T{}_2, J^T{}_3]\frac{\partial(g_2,g_3)}{\partial(u,v)}$$
$$\left.-\left((JJ^T)_{21}-(JJ^T)_{22}+(JJ^T)_{23}\right)[J^T{}_3, J^T{}_1]\frac{\partial(g_3,g_1)}{\partial(u,v)}\right\}/\det(JJ^T). \tag{24}$$

where $(JJ^T)_{ij}$ is the entry in the i-th row and j-th column of the matrix (JJ^T).

Notice that we have avoided the need to find the inverse of the matrix JJ^T, therefore the computation of drifts is much simpler. The formula given in eq(22) is a way to calculate dd(q) which is extremely convenient, (the examples in section VII will serve as an illustration, see later). Moreover, we should note here that the most important result in the theoretical sense is that equation (22) suggests that drift density is the projection of a linear combination of Lie brackets generated from J^T.

V. The Drift Density and the Self-Motion Manifold

The drift density defined in section III is a vector in space $\mathbb{R}^n$. Actually, the drift density is defined on the self-motion space, the self motion space has dimension equal to the degree of redundancy $r=n-m$. The drift density lies on the tangent space of the self-motion manifold. This tangent space has the dimension r. In this section we will find an r-dimensional chart of the self-motion manifold and find the expression for the drift density in the local coordinates.

Consider as before the kinematics of a redundant manipulator to be given by

$$x=K(q) \qquad | \; x\in\mathbb{R}^m \text{ and } q\in\mathbb{R}^n . \tag{25}$$

The self-motion space over x_o is defined as the solution set of the nonlinear equations $x_o=K(q)$,

$$Q_f=\{q\in\mathbb{R}^n \;|\; x_o=K(q)\}. \tag{26}$$

A point $q_f\in Q_f$ is called regular if the Jacobian $J=\partial x/\partial q$ is non-singular at the point q_f. If all the points in Q_f are regular, then the self-motion space Q_f is an (n-m) dimensional submanifold in the joint space. It has been proved by implicit mapping theorem on the manifold (see the proposition 6.2.1 in [5]), that Q_f being a manifold implies that we can always (locally) attach a chart to each point $q_f\in Q_f$. The chart u is an injection as $r<n$,

$$u: \; Q_f \rightarrow \mathbb{R}^r . \tag{27}$$

Thus each point q_f has one to one correspondence with $u=(u_1, \cdots, u_r)$ by $u=u(q_f)$, where $\{u_i\}$ is a set of orthogonal coordinate functions. Under the assumption of smooth manifold, any chart is a homeomorphism (see proposition 2.4.3 in [5]). Now our task is to find the homeomorphism u, to represent the self-motion manifold in a lower dimensional Euclidean space $\mathbb{R}^r$. This will be helpful for ascertaining the stability of drift motion using planar phase portrait technique.

One way to find the self-motion manifold is to integrate the tangent space (sometimes called the distribution of tangent vector fields). This method is commonly used to determine a curve by integrating its tangent vector. The existence of solutions of ordinary differential equations guarantees that a vector field is always integrable, but this is not always true for higher dimensional distributions. However it can be proven (using the same reasoning given in example 11.1.2 in [5], p.194) that the null space of J, ker J, is an integrable distribution on Q_f if the kinematic map $K:Q\rightarrow X\subset\mathbb{R}^m$ is a submersion (i.e., J is of full rank). In other words, at a nonsingular configuration q_f the null space ker J is integrable. Let $\{t_j^o\in\mathbb{R}^n \mid j=1, \ldots, r\}$ be the orthonormal basis vector fields for ker J. (The algorithms for computing $\{t_j^o\}$ are given in Appendix 1). Let the parameter u_j be the arc length of the curve that is generated from the

integration of t_j^o, such that,

$$\frac{\partial q}{\partial u_j} = t_j^o(q(u))$$

and hence,

$$q_f(u_j, u_j') = \int_0^{u_j} t_j^o(q_f(u))du_j \quad \text{with } u_j' \text{ being fixed.} \tag{28}$$

where $u=(u_1, \cdots, u_r)$, and u_j' is the (r-1)-tuple formed by deleting u_j from u. Then eq(28) establishes the local homeomorphism between point u and the configuration q_f.

The drift density given in eq(22) is a vector in $\mathbb{R}^n$ and can now be projected on to the chart u. The component of the projection on the coordinate u_i is a scalar, such that,

$$U_i(u) = U_i(u(q_f)) = \langle dd(q_f), t_i^o \rangle \quad \text{for } i=1, \cdots, r \ .$$

The other way around, the drift density $dd \in \mathbb{R}^n$ can be expressed as a decomposition based on the projection with respect to the chart u,

$$dd(u(q_f)) = \sum_{i=1}^{r} t_i^o(u)\, U_i(u) \ . \tag{29}$$

VI. Stability Analysis of Drift Motion

In this section we will determine the type of stability exhibited by the drift motion. The drift motion equilibrium set are those joint configurations at which the drift and hence the drift density is zero, i.e., dd(q)=0. Let these joint configurations be in the set $\mathcal{E}$, then,

$$\mathcal{E} = \{ q \in Q_f \mid dd(q)=0;\ x_0 = K(q) \} \ . \tag{30}$$

Recall in section IV that the drift density dd describes the rate of change of the drift motion occurring along the self motion space of x_0. Thus the drift density dd can be described by a constrained dynamical system (or descriptor system) as:

$$\dot{q}_f = dd(q_f) \quad | \quad x_0 = K(q_f) \ . \tag{31}$$

From section V, we know the drift density can be represented by the linear combination of the basis vectors of the null space of J, see equation eq(29). The left hand side of eq(31) can be rewritten as $\dot{q}_f = \sum_{i=1}^{r} \frac{\partial q_f}{\partial u_i} \dot{u}_i$. Hence we have,

$$\dot{u}_i = U_i \ , \quad \text{for } i=1, \ldots, r \ . \tag{32}$$

Now we are ready to state a stability theorem concerning the drift motion.

Theorem 1 : Let u be the chart for the self-motion manifold Q_f, that maps Q_f on to a subspace of $\mathbb{R}^m$, and U be the components of the projection of drift density dd on the tangent space of the chart u. Then the equilibrium point $q_e \in Q_f$ of the drift motion is an attractor [stable foci) in the neighborhood $||q-q_e|| < \epsilon$, if the matrix $[\frac{\partial U}{\partial u}]|_{q_e}$ is negative definite. O

Proof : Consider the Lyapunov function candidate, $V(q)=\frac{1}{2}dd^T dd$. The function $V(q)$ is positive definite in some neighborhood of q_e because $V(q)$ has partial derivative about q, $V(q_e)=0$, and $V(q)>0$ everywhere except at q_e. Let us denote the vector $U=[U_1, \cdots, U_r]^T$ and denote the matrix $N_J=[t_1^o \cdots t_r^o]$. Equation (29) can be rewritten as $dd=N_J U$. Then the Lyapunov derivative is:

$$\dot{V}=dd^T\dot{dd}=U^T [t_1^o, \cdots, t_r^o]^T([\dot{t}_1^o, \cdots, \dot{t}_r^o] U + [t_1^o, \cdots, t_r^o] \dot{U})$$

We claim that, $[t_1^o, \ldots, t_r^o]^T [\dot{t}_1^o, \cdots, \dot{t}_r^o] = [0]\in\mathbb{R}^{r\times r}$. This is because, for every i, $\frac{d}{dt}(||t_i^o||^2)=0$ implies that $<t_i^o,\dot{t}_i^o>=0$ and, for $i\neq j$, $<t_i^o,t_j^o> = 0$ implies that $<t_i^o,\dot{t}_j^o> = 0$, since for all i, t_i^o are the orthonormal basis vectors. Also we notice that $[t_1^o, \cdots, t_r^o]^T [t_1^o, \cdots, t_r^o] = I$,, where I, stands for an r by r identity matrix.

Using the notation that $[\frac{\partial U}{\partial u}]$ is a matrix $[\frac{\partial U_i}{\partial u_j}]\in\mathbb{R}^{r\times r}$, finally we arrive at

$$\dot{V}=U^T \dot{U}=U^T \sum_{j=1}^{m}\frac{\partial U}{\partial u_j}\dot{u}_j=U^T \sum_{j=1}^{m}\frac{\partial U}{\partial u_j}U_j =U^T [\frac{\partial U}{\partial u}] U \ . \qquad (33)$$

Therefore the eigen-structure of the differential map dU of the drift density determines the behavior of the drift motion around the equilibrium point. The equilibrium point $q_e\in Q_f$ is asymptotically stable if $\sigma(\frac{\partial U}{\partial u})\in C_0^-$ or $[\frac{\partial U}{\partial u}]$ is negative definite at q_e. Where $\sigma([\frac{\partial U}{\partial u}])$ is the eigen value set of matrix $[\frac{\partial U}{\partial u}]$ and, C_0^- denotes the complex left half plane. This completes the proof. ■

Drift Phase Portrait for visualization

Based on Theorem 1 we can analyze the stability of the drift motion for two degree of redundancy robot manipulators using the phase portrait method. The phase portrait techniques provide a powerful tool for visualization of the drift trajectories and their stability.

The basis for the stability analysis involving the phase portrait method is the **Hadamard-Perron Theorem**[17], which tells us that in the neighborhood of a hyperbolic **fixed** point † the **stable/unstable** manifold of the map ϕ is tangent to the **stable/unstable subspace** of the differential map $d\phi$. Additionally, for non-hyperbolic fixed point, the "Center Manifold **Theorem**"[9], informs us that there exists a center manifold (which is not necessarily unique) tangent to the eigen-space corresponding to the zero real part eigenvalue of the differential map $d\phi$. Furthermore, for those systems with empty unstable manifold (real part of the system eigenvalues are non-positive), the "Reduction **Principle**"[9] allows us to determine the overall stability from the stability of the reduced system. Following these well established results, the local stability of the drift map (5) can be characterized by the phase portrait of the differential map (31).

The formal definitions of the phase portrait and the conditions for equivalency of two phase portraits **(p.35,[17])** are given in Appendix 2. The definition of the types of equilibrium points found in the phase portrait are also included in the appendix for easy readability.

† **For a continuous system $\dot{x}=f(x)$ the hyperbolic fixed point is the critical point where the Jacobian $Df(x)$ has no eigen values with zero real** part.

VII. Simulations

In this section we give two examples to illustrate the use of drift density. The first example has work space dimension of $m=3$ and the degree of redundancy $r=1$. In the second example, the work space dimension is m=2 and the degree of redundancy is $r=2$.

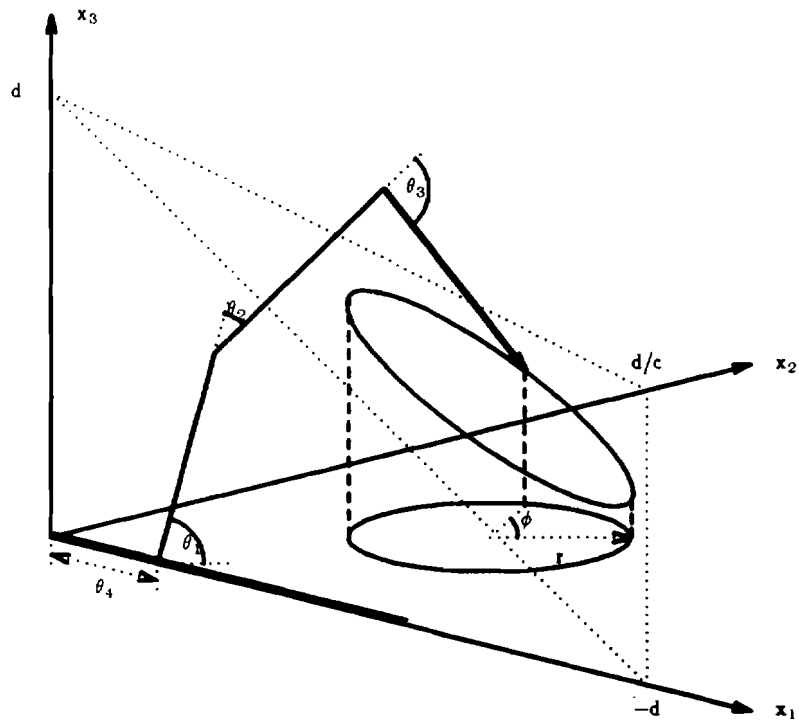

Fig.1 Robot in Example 1, n=4, m=3, and r=1

Example 1 (with $n=4, m=3, r=1$):

In this example we consider a four link manipulator with the first joint being prismatic, the remaining three have **revolute** joints (see **Fig.1**). The equations of motions of the manipulator in Cartesian space (x_1,x_2,x_3) is given by $x=K(q)$:

$$x_1=q_4=\theta_4, \qquad x_2=\sum_{i=1}^{3} l_i \cos q_i \quad \text{and} \quad x_3=\sum_{i=1}^{3} l_i \sin q_i \ , \qquad \text{with} \quad q_i=\sum_{j=1}^{i}\theta_j \ , \quad i=1,\cdots,3.$$

where for $i=1,\ldots,4$, θ_i represent the angular or radial motion of the joint i, and l_i is the length of link i which has **revolute** joint. The manipulator is to trace a closed curve which is formed by the intersection of a plane and a cylinder of radius of r. The cylinder axis is parallel to the x_3 axis, and the plane cuts axes x_1,x_2 and x_3 at $-d, d/c$ and d respectively. The equation of the closed path in the work space can be parameterieed in terms of a parameter 4, such that

$$x_1=a+r\cos\phi, \quad x_2=b+r\sin\phi, \quad \text{and,} \quad x_3=(x_1+cx_2)-d \ ,$$

where a,b,c,d and r are constants which determine the position and siee of the path. As mentioned above, the constant c determines the intersection points of the plane with the three

axes x_1, x_2 and x_3. The radius r determines the loop size of the path. The other constant a, b, and d are chosen to place the end effector of the initial joint configuration $\theta(0)$ on the path. In the simulations we chose c=2 and r=0.2. In Fig.2 and Fig.3 we choose $\theta(0)=(1, 0.5, -1.2, 0.2)$ in their respective unit (radians and meters).

We notice that in this particular example the fiber over $x_o=(0.2, 1.24, -1.86) = K(\theta(0))$ is such that the two self motion arcs corresponding to two different manipulator configurations are connected into one.

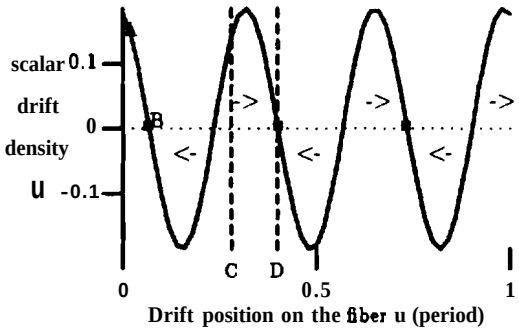

Fig.2a Phase portrait (n=4, m=3, r=1)

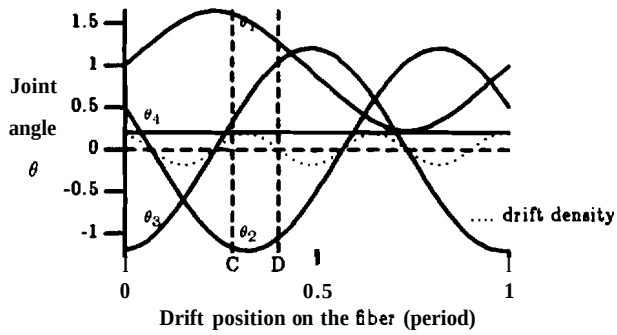

Fig.2b Joint motion

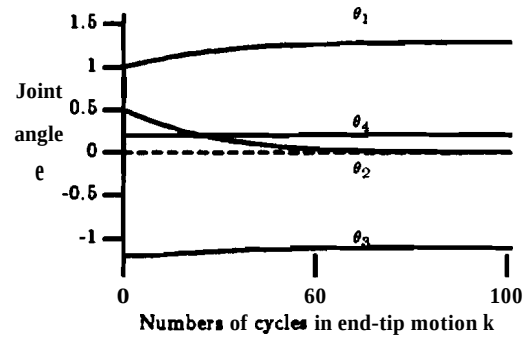

Fig.3a Motion of states (from point A to B)

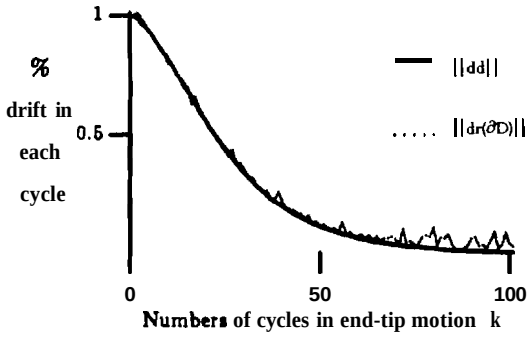

Fig.3b Convergence of the drift (from point A to B)

In Fig.2a, the phase portrait of the drift motion is shown. The horizontal axis u is the arc length on the self-motion manifold (position on the fiber), it is calculated from the integral of the tangent vector t° given by the algorithm described in Appendix 1. The arrows shown in Fig.2a indicate the direction of motion along the fiber for particular configuration. The vertical axis U=<dd,to> represents the scalar drift density. The joint angle versus the position on the fiber is shown in Fig.2b, also marked on the figure are the various equilibrium joint angles. The time history of the joint motions versus the number of times around the work space loop is shown in Fig.3a, when the initial joint configuration is $\theta(0)=(1.6, -1.16, 0.3, 0.2)$ radians (corresponding to point A in Fig.2a). The amount of the drift in each cycle of the loop (at the position x_o) as the

joints drift from position A to B is shown in Fig.3b. The measures of the drift shown in Fig.3b is computed from the norm of the vectors dd and $dr(\partial D)$, i.e., $||dd||$ and $||dr(\partial D)||$. We can see from Fig.2a that the scalar drift density is zero at configuration B, and it is in fact a stable equilibrium point. If the initial configuration of the joints $\theta(0)$ is at A then the final joint configuration will end up with configuration B. Hence, the drift density measure shown in Fig.3b indeed goes to zero as the joint configuration drifts from point A to B. If the initial configurations are at point C (with their corresponding joint angles as shown in Fig.2b), we can see that the joints will drift to the stable equilibrium point D. Indeed the phase portrait Fig.2a indicates that the configuration D is drift stable. The motion of the joints from the initial configurations C to the final configuration D is shown in Fig.4a and Fig.4b. The joint configuration versus the number of times around the workspace loop is shown in Fig.4a, the measure of the drift velocity is also shown in Fig.4b.

From these simulations we can conclude that the drift density measures indicate accurately the behavior of the drift motion. Furthermore the scalar drift density and the position on the fiber is useful for creating the phase portrait which reveals the trajectories of the drift motions.

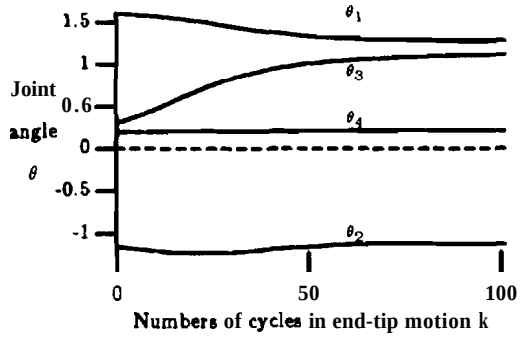

Fig.4a Motion of states (from point C to D)

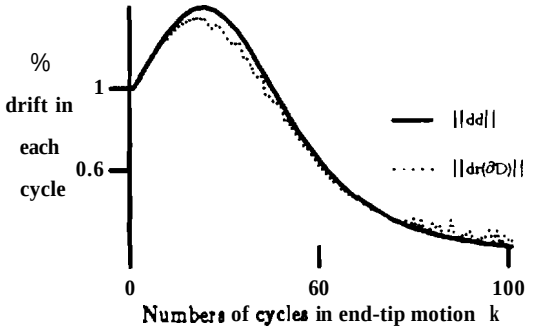

Fig.4b Convergence of the drift (from point C to D)

Example 2 (with n=4, m=2, r=2):

Now consider a four-link (n=4) planar manipulator with unit link lengths. The tip of the manipulator moves on a planar workspace (m=2), here the degree of redundancy is two. The joint angles θ_1, θ_2, θ_3 and θ_4 are related to the angles q_1, q_2, q_3 and q_4 as, $q_k=\sum_{i=1}^{k}\theta_i$. Then, the Jacobian J with respect to q is given by

$$J=\begin{bmatrix} -s_1 & -s_2 & -s_3 & -s_4 \\ c_1 & c_2 & c_3 & c_4 \end{bmatrix},$$

with $s_i=\sin(q_i)$ and $c_i=\cos(q_i)$. The actual drift is found by integrating $\dot{q}$ over the closed loop path in the workspace given by eq(4). Gear's ordinary differential equation eolver is used to carry out the integration.

The end effector of the manipulator is required to trace a square of dimension 0.25m by 0.25m in the counter-clockwise direction. The vertex of the square is $x_o=K(\theta(0))$, with $\theta(0)=(-1.5,-1.0,1.0,1.5)$ radians. The phase portrait of this manipulator is shown in Fig.5. First notice that point A is a saddle point, point B and B' are stable nodes. Point C is an unstable node and point D is a saddle-node point, notice that around the point D the trajectories have similar structure as that of the origin in **Fig.A1** (see Appendix 2).

Fig.6 shows the time history of the drift motion from another initial joint configuration $\theta(0)=(-1.5,-1.0,1.0,1.5)$ radians, corresponding to the point S' in the phase portrait Fig.5 to the second stable limit point B' in the phase portrait.

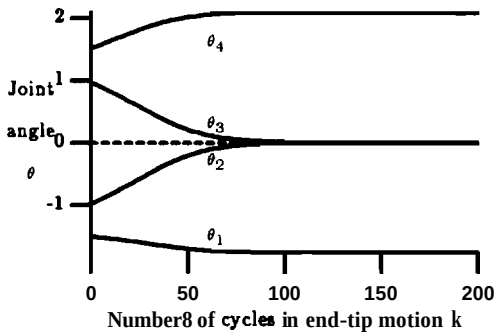

Fig.6a Motion of states (from point 9' to B')

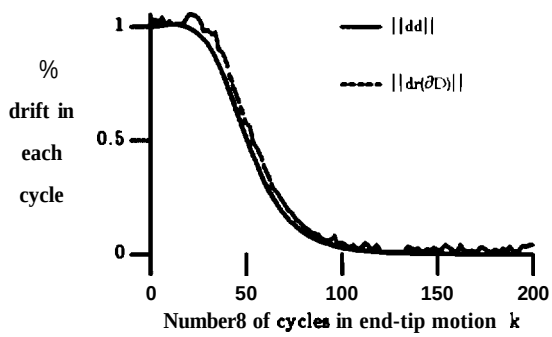

Fig.6b Convergence of the drift (from point S' to B')

In **Fig.7a** we show the evolution of the joint angles from point S with $\theta(0)=(-0.6,-2.07,1.96,-1.24)$ radians to the final configuration $\theta=(0.3,-2.13,0,0)$ radians, corresponding to point B. From the phase portrait we see indeed that the trajectory from point "S" does end up on point "B", which is what we can expect in **Fig.7a.**

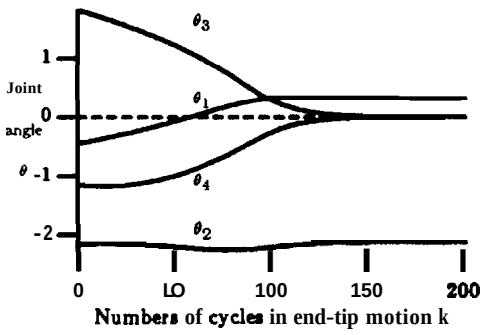

Fig.7a Motion of states (from point 9 to B)

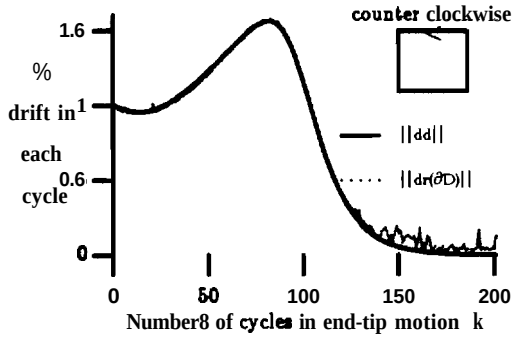

Fig.7b Convergence of the drift (from point S to B)

Klein and **Kee[11]** observed that if the direction of the path in the workspace is reversed the drift motion of the manipulator changes. From the definition of drift in **eq(6)** and the drift density in **eq(18)** we can see that reversing the path direction will reverse the sign of the integral and the sign of drift density. The drift phase portrait will change correspondingly, and the

source nodes in the phase portrait will become drain nodes, and vice-versa as the phase portrait trajectories change their directions. From the drift phase portrait shown in Fig.5 we can see that the point C' is now a stable node for clockwise motion. The drift motion starting from point S will converge to point B for counter clockwise path, and will converge to point C' for clockwise path. This clearly shows why different path direction produces different drift motion. Further this explains and illustrates why drift stable configurations become unstable configurations and drift unstable configurations become stable configurations on reversal of the path direction.

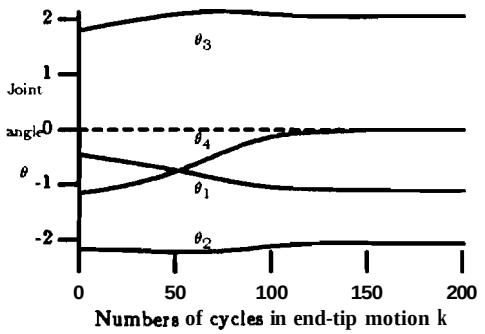

Fig.8a Motion of states (from S to C')

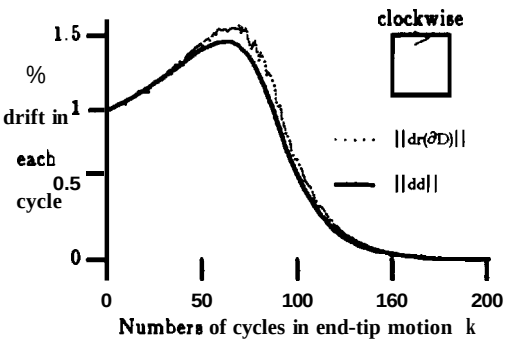

Fig.8b Convergence of the drift (from S to C')

As a final note, we see the critical point joint configurations can be analytically found by setting the drift density vector to zero, i.e., dd=0. In this example we have,

$$N_J^T = \begin{bmatrix} s_{32} & -s_{31} & s_{21} & 0 \\ s_{42} & -s_{41} & 0 & s_{21} \end{bmatrix} \quad \text{and the Lie bracket } [J^T_1, J^T_2] = [1\ 1\ 1\ 1]^T$$

here we have denoted $s_{ji} = \sin(q_j - q_i) = \sin(\sum_{k=1}^{j} \theta_k - \sum_{k=1}^{i} \theta_k)$. From (23) we see,

$$dd\,|_{m=2} = N_J N_J^T [J^+_1, J^+_2] = N_J \begin{bmatrix} (s_{32}+s_{13}+s_{21}) \\ (s_{42}+s_{14}+s_{21}) \end{bmatrix} / \det(JJ^T) \qquad (34)$$

setting the elements of dd to zero we obtain the critical point conditions as,

case 1 θ_2 and $\theta_3 = 0$; (35)

case 2 θ_3 and $\theta_4 = 0$; (36)

case 3 $\theta_4 = 0$ and $\theta_2 + \theta_3 = 0$. (37)

(Notice that it is significantly simpler to calculate these critical points by setting dd=0, using the method described in this paper, than using the Lie bracket condition on J+, described in [15].) From the simulations shown in Fig.6a and Fig.7a we see in the stable configuration the condition given by (35) and (36) respectively are indeed verified. Further the result shown in Fig.8a confirms the condition given by (37). Notice again the stability of the the drift about these critical point were obtained from the phase portrait analysis.

VIII. Conclusion

In this paper the joint drift motion of the redundant robots under pseudo-inverse Jacobian control has been studied. The drift phenomenon is in fact the result from the non-holonomity. In order to study this phenomenon we proposed a measure of the drift for kinematically redundant robots. This measure was used to determine the local stability of joint drift under pseudo-inverse Jacobian control. Using Lyapunov stability analysis techniques drift stable configurations could be characterized by analyzing the motion in the self-motion manifold. A drift phase portrait was then constructed for robots with two or less degrees of redundancy. It was then possible to visualize the drift stable joint configurations and the unstable configurations. The effects of workspace path reversal on the drift stable/unstable configuration were also clearly seen from the drift phase portraits. The zero drift configurations of the manipulator could be obtained by setting $dd(q)=0$. However the stability of those joint configurations were specified by the eigenvalues of $[\frac{\partial U}{\partial u}]$, from Theorem 1. It is therefore possible that some manipulator configurations for a given x_o will exhibit repulsive, attractive or of saddle node type characteristics. We have seen all three from the simulations. However there may exist some self-motion manifolds of some particular x_o for which drift is always non zero, i.e., $dd \neq 0$, in which case drift may not have a limit[11]. Further investigation needs to be carried out; to determine the class of geometries, locations and size of the loop which result in $dd \neq 0$, for all q. The effect of the workspace loop size on the drift motion also needs to be investigated further. We have also observed on the phase portrait (for $r>1$) that the bifurcation of the joint trajectories (non-hyperbolic critical point) do occur, (see point E on the phase portrait in Fig.5). In the neighborhood of these critical points the behaviors of the joint motion is extremely sensitive to the initial conditions. This leads us to suspect that chaotic motion could possibly occur for high degrees redundancy $(r>1)$ and certain manipulator geometric structures. This is because non-integrable dynamical systems can exhibit chaotic motion[14].

Appendix 1: Calculating the Null Space of the Jacobian J

Let J be an m by n matrix. Let the j-th column of the transpose matrix J^T be denoted by J^T_j , the null space of J be denoted by ker J, and the basis vector of ker J be denoted by ν_j. Then the algorithms for computing the basis of the null space of J are given as follows.

Algorithm 1 : If $m=n-1$, then the basis vector $\nu \in \mathbb{R}^n$ is

$$\nu = {}^*(J^T_1 \wedge \cdots \wedge J^T_{n-1}). \qquad (A1.1)$$

where the symbol A is used to denote the "wedge product" operation, and ${}^*W_m$ is used to denote the "adjoint of the multi-vector of degree m" . Here the m-vector W, is given by $W_m=(J^T_1 \wedge \cdots \wedge J^T_{n-1})$, where $m=n-1$.

By definition of the adjoint of W_m the components of ν are[6],

$$\nu_i=(-1)^{i-1}W^{i'}_m, \qquad i=1,...,n.$$

where i' is an (n-1)-tuple made after deleting the number i from $(1,...,n)$, and $W^{i'}_m$ is the component of W, with superscript i'. This **adjoint** of the m-vector ν has the following **properties**[6]: (1) ν is a vector normal to the $(n-1)$ space spanned by $J^T_1, \cdots, J^T_{n-1}$; (2) $(\nu, J^T_1, \cdots, J^T_{n-1})$ is a positively oriented frame in $\mathbb{R}^n$; (3) $||\nu||=||W_m||$.

These properties are the necessary conditions of the null space basis vector. The component of $W_{,,,}$ can be found from equation (6-13a) **in**[6]

$$W^{i'}_m=J\binom{i'}{\lambda} \qquad | \lambda=(1, \cdots, m).$$

where, $J\binom{i'}{\lambda}$ is the **(n-1)th** order minor of J as discussed in the section IV. Thus the null space of the Jacobian of any manipulator with one degree of redundancy can be computed as given in the above. As an example in **n=4, m=3,** we have,

$$\nu=[\ J\binom{1,2,3}{2,3,4}, -J\binom{1,2,3}{1,3,4}, J\binom{1,2,3}{1,2,4}, -J\binom{1,2,3}{1,2,3}\ ]^T \tag{A1.2}$$

Algorithm 2 : For **n=4, m=2,** the basis vectors $\nu\in\mathbb{R}^n$ can be computed by

$$\nu_1=[\ J\binom{1,2}{2,3}, -J\binom{1,2}{1,3}, J \quad , \mathbf{0}, J]^T \text{ and }$$

$$\nu_2=[\ J\binom{1,2}{2,4}, -J\binom{1,2}{1,4}, \mathbf{0}, J \quad]^T . \tag{A1.3}$$

These formulas are derived in terms of conventional matrix technique for finding the basis vectors of a linear subspace. Furthermore the orthonormal bases can be found by Gram-Schmidt orthogonalization method, which yields:

$$t^o_u=\nu_1/||\nu_1|| ; \qquad t_v=\nu_2-\nu_1<\nu_1,\nu_2>/||\nu_1||^2$$

$$t^o_v=t_v/||t_v|| .$$

Then, ker **J=span**(t^o_u, t^o_v) , the inner product $<t^o_u, t^o_v>=0$ and $||t^o_u||=1$ and $||t^o_v||=1$. Thus t^o_u and t^o_v is the pair of orthonormal bases of the null space of ker J.

Appendix 2: Critical Points on the Phase Portrait

Definition A2.1 : Let Φ be an r-times differentiable vector field defined on the manifold M $(r\geq 1)$. The set of all the oriented orbits $\hat{\gamma}(t)$ of Φ is called the ***phase portrait*** of Φ, and is denoted by $P(\Phi,M)$.

Definition A2.2 : Let M_1, M_2 be manifolds and let Φ_i be the r-times differentiable vector field defined on the manifold M_i, for $i=1,2$, $(r\geq 1)$. The fields Φ_1 and Φ_2 are said to have ***equivalent phase portraits*** iff there **exists** a homeomorphism h of M_1 onto M_2 such that

$$\hat{\gamma}\in P(\Phi_1,M_1) \quad \text{iff} \quad h(\hat{\gamma})\in P(\Phi_2,M_2) . \tag{A2.1}$$

Following diagram illustrates the condition for the equivalency of the two phase portraits.

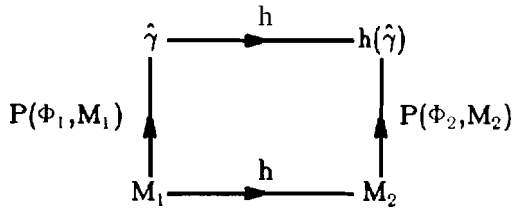

Orbits

Phase Portrait

Manifold

Let M_1 be the r-dimensional self-motion manifold in $\mathbb{R}^n$, and M_2 be the subspace in $\mathbb{R}^r$. We may find a homeomorphism h that maps M_1 to M_2. If we use the same homeomorphism h for mapping the orbits on M_1 to the orbits on M_2, then we are able to obtain a planar graph $P(\Phi_2,M_2)$ that is equivalent to the phase portrait $P(\Phi_1,M_1)$ on the manifold in high dimensional space. For our simulation we will use the arc-length as h for r=1, and integrate the null space vectors of the Jacobian as h for r=2.

Types of Critical Points Found in Phase Portrait

In order to distinguish between the various types of critical (equilibrium) points of the system on $\mathbb{R}^2$ [13].

Consider the below nonlinear system,

$$\dot{x}=f_1(x,y)$$

$$\dot{y}=f_2(x,y)\,. \qquad \text{(A2.2)}$$

We assume the equilibrium point of eq(A2.2) is an isolated critical point. Let the matrix of the linearized system be $A=\frac{\partial(f_1,f_2)}{\partial(x,y)}$. If A is nonsingular (no eero eigenvalue) the critical point of the system eq(A2.2) is hyperbolic. The hyperbolic critical point is either a node, center, focus or saddle, these are some commonly occurring critical points. The Hartman-Grobman Theorem [1] shows that near a hyperbolic critical point the orbit structure of a nonlinear system is qualitatively the same, (in the sense of being topologically conjugate), as the orbit structure given by the associated linearieed system. When at least one of the eigenvalues of A is eero, the critical point is called a non-hyperbolic point. The trajectories in the neighborhood of a non-hyperbolic critical points can be very varied. We illustrate some of these trajectories, a saddle-node is shown in Fig.A1, a critical point with an elliptic domain is shown in Fig.A2 and a cusp is shown in Fig.A3.

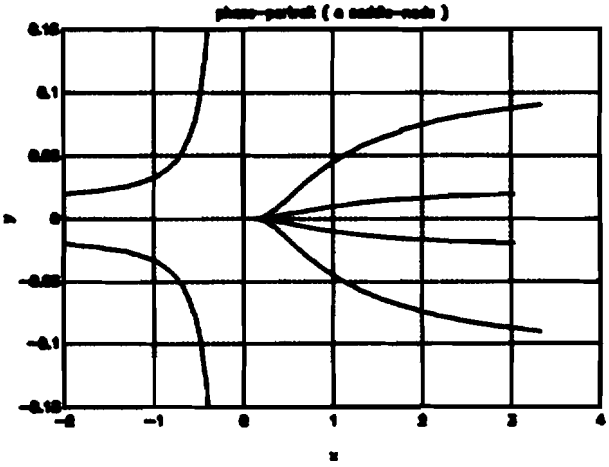

Fig.A1 A saddle-node

$\dot{x}=-x^2$

$\dot{y}=-y$

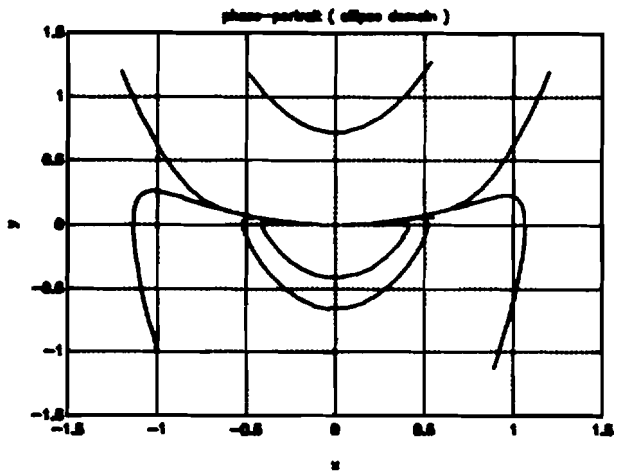

Fig.A2 A critical point with ellipse domain

$\dot{x}=y$

$\dot{y}=-x^3+4xy$

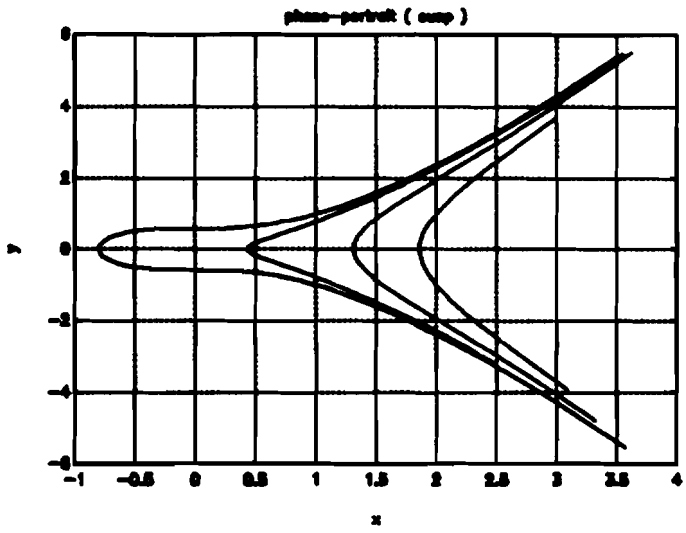

Fig.A3 A cusp

$\dot{x}=y$

$\dot{y}=x^2$

The following theorems from Arnold indicate that the form of the nonlinear dynamical system equation will reveal the type of critical points that can occur on the phase portrait. The proofs of these theorems can be found in (p.340, pp.357-362, [1]).

Theorem *A2.1* (Arnold): [Critical point with one sero eigen-value case]

Consider the system eq(A2.2) with detA=0 and trA≠0, so it has the nominal form as,

$$\dot{x}=p(x,y)\,,$$

$$\dot{y}=y+q(x,y)\,.$$

Define the function $\phi(x)$ as $y=\phi(x)$ | $\phi(x)+q(x,\phi(x))=0$, and assume that the function p can be expanded as

$$p(x,\phi(x))=a_m x^m+a_{m-1}x^{m-1}+\cdots\cdots,\quad \text{where } x\in \text{open set of } 0$$

Then the type of the critical point can be obtained from Table.1 .

m a_m	*odd* *>0*	*odd* *<0*	*even*
	node	saddle	saddle-node

Table.1 Non-hyperbolic critical points (One cero eigenvalue case)

Theorem A2.2 (Arnold): [Critical points with two zero eigen-values case]

Consider the system eq(A2.2) with $\det A=0$, $\mathrm{tr}A=0$ and $A\neq 0$, so it has the nominal form as,

$$\dot{x}=y\ ,$$

$$\dot{y}=ax^k(1+h(x))+bx^n y(1+g(x))+y^2R(x,y)\ ,$$

where, $h(x)$, $g(x)$ and $R(x,y)$ are smooth in a neighborhood of the origin, $h(0)=g(0)=0$, and $k\geq 2$, also $a\neq 0$ and $n\geq 1$. Then the type of the critical point can be obtained from Table.2 and Tabie.3.

For k even , $(k=2m)$

$b=0$	$b\neq 0$ $n\geq m$	$b\neq 0$ $n<m$
cusp	cusp	saddle-node

Table.2 Non-hyperbolic critical points (two zero eigenvalue case)

For k odd, $(k=2m+1)$, $X:=b^2+4(m+1)a$

$a>0$	$a<0$						
	$b=0$	$b\neq 0$		$b\neq 0$			
				n=even		n=odd	
		$n>m$	$n=m$ $\lambda<0$	$n<m$	$n=m$ $\lambda\geq 0$	$n<m$	$n=m$ $\lambda\geq 0$
saddle	focus or center			node		ellipse domain	

Table.3 Non-hyperbolic critical points (two rero eigenvalue case)

Arnold's theorem allows us to determine the nature of the phase portrait we expect to observe if we have prior knowledge of the analytical form of the nonlinear dynamical systems. We will observe these phase portrait phenomena in our drift phase portrait, however we will discover them from numerical experiments as the analytical expression of the drift density and the position on the fiber are not available.

References

1. V.I. Arnold, "Geometrical Methods in the Theory of Ordinary Differential Equations," in *New York: Springer-Verlag, 1083.*
2. J.S. Bay, "An Approximate Poincare Return Map for the Dynamics of Drifting Manipulators under Pseudo-inverse Control," *IEEE International Conference on System Engineering, pp.19-16, Aug. 9-11, 1990.*
3. A.M. Bloch and N.H. McClamroch, "Control of Machanical systems with Classical Nonholonomic Constraints," *Proceedings of the 28th Conference on Decision and Control, Tampa, Florida, pp.201-205, 1080.*
4. W.A. Boothby, "An Introduction to Differentiable Manifolds and Riemanian Geometry ," in *dnd edition, Orlando: Academic Press, 1986.*
5. F. Brickell and R.S. Clark, "Differentiable Manifolds: An Introduction," in *London: V.N. Reinhold Company, 1070.*
6. W.H. Fleming, "Functions of Several Variables," in *Reading, Massachussets: Addidon-Wedley Publishing Company, Inc., 1965.*
7. F.R. Gantmacher, "The Theory of Matrices Vol.1," in *New York: Chelsea Publishing Co., 1060.*
8. H. Grunsky, "The General Stokes' Theorem," in *Borton, MA: Pitman Publishing Inc., 1983.*
9. A. Isidori, "Nonlinear Control Systems," in *dnd Ed. New York: Springer-Verlag, 1080.*
10. C.A. Klein and C.H. Huang, "Review of Pseudo-inverse Control for Use with Kinematically Redundant Manipulators ," *IBEB Transactions on System, Man and Cybernetics, V.SMC-13, pp.245-250, 1083.*
11. C.A. Klein and K.B. Kee, "The Nature of Drift in Pseudo-inverse Control of Kinematically Redundant Manipulators ," *IBEB Tranractionr on Roboticr ond Automation, V.RA-5. pp291-294, 1080.*
12. S. Luo and S. Ahmad, "Measure of Joint Path Drift for Kinematically Redundant Robots," *Proc. 1991 IEEE International Conference on Roboticr and Automation, Sacramento, CA. pp.1163-1168, 1991.*
13. L. Perko, "Differential Equations and Dynamic Systems," in *New York: Springer-Verlag, 1991.*
14. S.N. Rasband, "Chaotic Dynamics of Nonlinear Systems," in *New York: Jobn Wiley & Sons, 1000.*
16. T. Shamir and Y. Yomdin, "Repeatability of Redundant Manipulators: Mathematical Solution of the Problem," *IEEE Transactions on Automatic Control, V.AC-33, pp.1004-1009, 1088.*
16. M. Spivak, "Calculus on Manifolds," in *New York: Benjamin, 1965.*
17. W. Sslenk, "An Introduction to the Theory of Smooth Dynamical Systems," in *Chicherter: John Wiley & Sons, 1984.*

m	
a_m	<0
	node saddle saddle-node

Table.1 Non-hyperbolic critical points (One **zero** eigenvalue case)

Theorem ***A2.2*** (Arnold) : [Critical points with two **zero** eigen-values case]

Consider the system eq(A2.2) with **detA=0, trA=0** and **A≠0,** so it has the nominal form as,

$$\dot{x}=y\ ,$$

$$\dot{y}=ax^k(1+h(x))+bx^n y(1+g(x))+y^2R(x,y)\ ,$$

where, $h(x)$, $g(x)$ and $R(x,y)$ are smooth in a neighborhood of the origin, $h(0)=g(0)=0$, and $k\geq 2$, also $a\neq 0$ and $n\geq 1$. Then the type of the critical point can be obtained from Table.2 and Table.3.

For k even , $(k=2m)$

$b=0$	$b\neq 0$ $n\geq m$	$b\neq 0$ $n<m$
cusp		saddle-node

Table.2 Non-hyperbolic **critical** points (two **zero** eigenvalue **case)**

For k odd, $(k=2m+1)$, $\lambda:=b^2+4(m+1)a$

$a>0$	$a<0$					
	$b=0$	$b\neq 0$		$b\neq 0$		
				n=even	n=odd	
		$n>m$	$n=m$ $\lambda<0$	$n<m$	$n=m$ $\lambda\geq 0$	$n<m$	$n=m$ $\lambda\geq 0$
saddle	focus or center			node		ellipse domain	

Table.3 Non-hyperbolic **critical** points (two **zero** eigenvalue **case)**

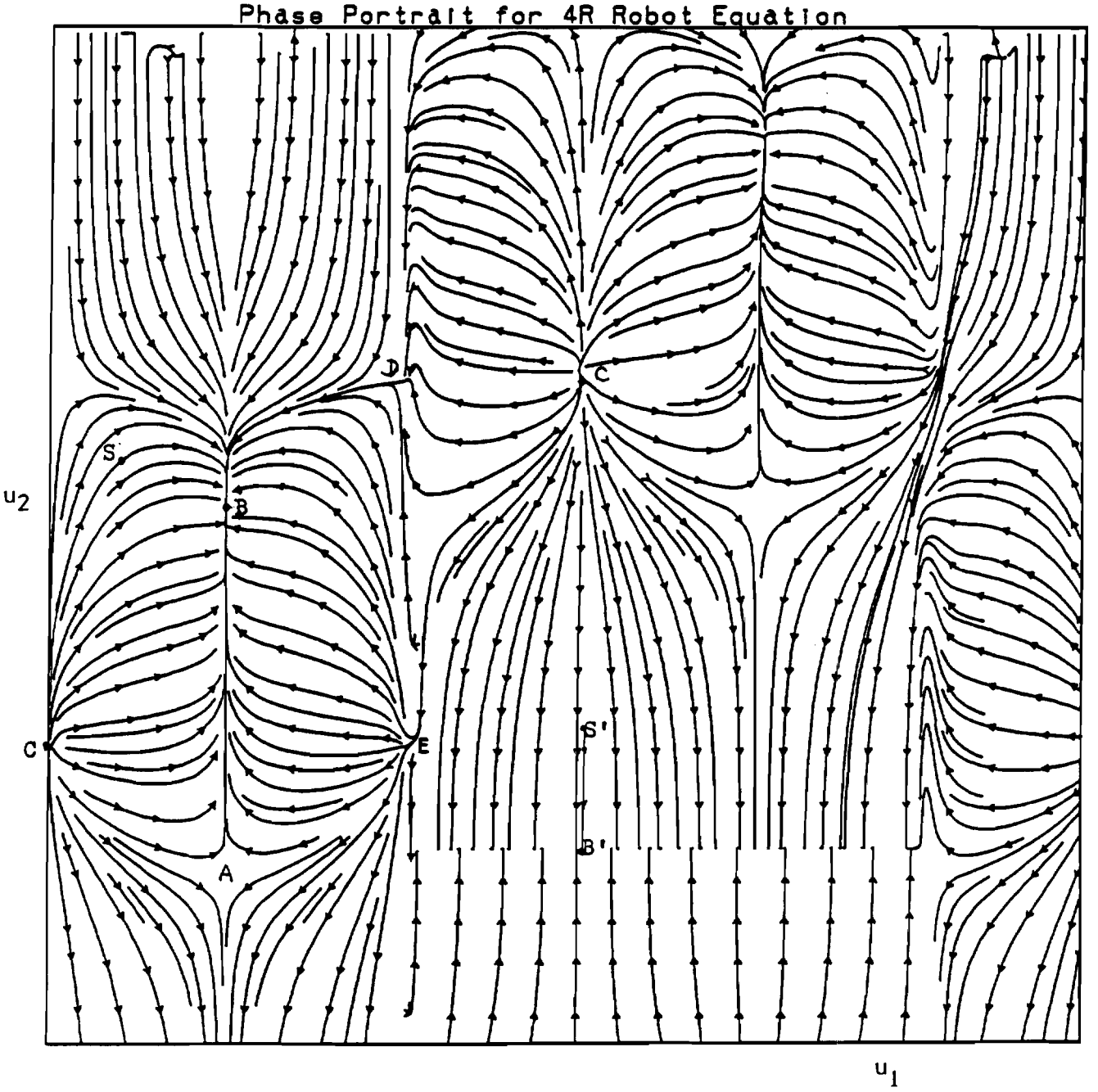

Fig. 5 Phase Portrait (n=4, m=2, r=2)